ISSN 0957-4484

NANOTECHNOLOGY

VOLUME 22 NUMBER 4 28 JANUARY 2011

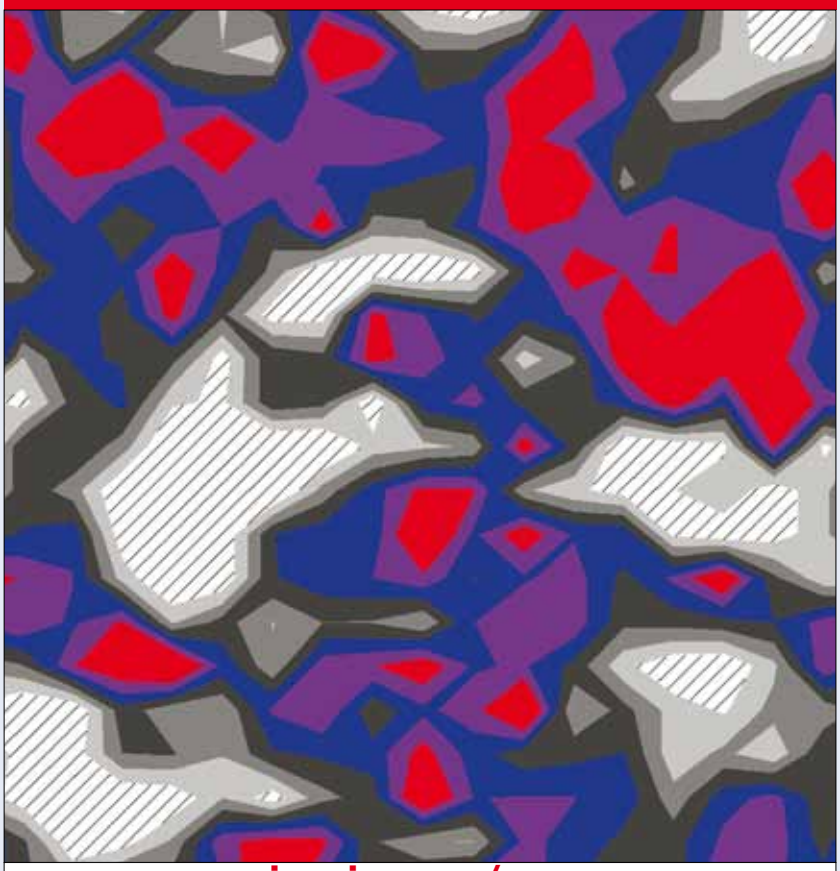

iopscience.org/nano

Featured article

A study of graphene films synthesized on nickel substrates: existence and origin of small-base-area peaks

Y H Kahng, S Lee, M Choe, G Jo, W Park, J Yoon, W-K Hong, C H Cho, B H Lee and T Lee

IOP Publishing

Nanotechnology **22** (2011) 045706 (9pp) doi:10.1088/0957-4484/22/4/045706

A study of graphene films synthesized on nickel substrates: existence and origin of small-base-area peaks

Yung Ho Kahng[1,2,4], Sangchul Lee[3], Minhyeok Choe[1], Gunho Jo[1], Woojin Park[1], Jongwon Yoon[1], Woong-Ki Hong[1,5], Chun Hum Cho[3], Byoung Hun Lee[1,3] and Takhee Lee[1,3,4]

[1] Department of Materials Science and Engineering, Gwangju Institute of Science and Technology, Gwangju 500-712, Korea
[2] Research Institute for Solar and Sustainable Energies, Gwangju Institute of Science and Technology, Gwangju 500-712, Korea
[3] Department of Nanobio Materials and Electronics, Gwangju Institute of Science and Technology, Gwangju 500-712, Korea

E-mail: yhkahng@gist.ac.kr and tlee@gist.ac.kr

Received 11 August 2010, in final form 11 October 2010
Published 20 December 2010
Online at stacks.iop.org/Nano/22/045706

Abstract
Large-area graphene films, synthesized by the chemical vapor deposition (CVD) method, have the potential to be used as electrodes. However, the electrical properties of CVD-synthesized graphene films fall short of the best results obtained for graphene films prepared by other methods. Therefore, it is important to understand the reason why these electrical properties are inferior to improve the applicability of CVD-grown graphene films. Here, we show that CVD-grown graphene films on nickel substrates contain many small-base-area (SBA) peaks that scatter conducting electrons, thereby decreasing the Hall mobility of charges in the films. These SBA peaks were induced by small peaks on the nickel surface and are likely composed of amorphous carbon. The formation of these SBA peaks on graphene films was successfully suppressed by controlling the surface morphology of the nickel substrate. These findings may be useful for the development of a CVD synthesis method that is capable of producing better quality graphene films with large areas.

S Online supplementary data available from stacks.iop.org/Nano/22/045706/mmedia

(Some figures in this article are in colour only in the electronic version)

1. Introduction

Since its discovery in 2004, graphene has attracted tremendous interest due to its advantageous material properties, including high charge mobility, transparency, mechanical strength and flexibility [1, 2]. Accordingly, graphene is expected to play a crucial role as a transparent and conductive electrode in next-generation electronic devices [3]. Already, pioneering studies have reported the application of graphene as electrodes in liquid crystal displays [4], organic memories [5], organic field-effect transistors [6–8], light-emitting diodes [9–12] and organic solar cells [13–17]. For successful applications, graphene needs to be prepared in large-area films of high material quality. Currently, large-area graphene films are prepared by solution-based processes [18–20] or chemical vapor deposition (CVD) onto catalytic metal surfaces [21–34]. Among these products, CVD-grown graphene films typically show approximately one order of magnitude less sheet resistance than solution-processed graphene films, making them more attractive for application in high-performance electronic device [3].

However, even CVD-grown graphene film shows significantly higher sheet resistance (300–1000 Ω/□) than indium

[4] Authors to whom any correspondence should be addressed.
[5] Present address: Nanoscience Centre, University of Cambridge, Cambridge CB3 0FF, UK.

tin oxide (ITO) film (10–30 Ω/□), which is the current standard material for industrial transparent electrodes [3]. In addition, the mobility of CVD-graphene is in the range of a few hundred $cm^2\ V^{-1}\ s^{-1}$ [24, 27]. These inferior electrical properties of CVD-grown graphene films compared to ITO films have restricted the applications of graphene, preventing it from being used for a wide array of potential applications. For example, the higher sheet resistance is the critical reason why graphene-electrode organic solar cells have shown power conversion efficiencies of less than 2% [13–17]. In contrast, the efficiencies of ITO-electrode organic solar cells have exceeded 6% [35–37]. Given that the observed electrical properties of graphene are far below predicted limits, including a theoretically achievable sheet resistance of 10–30 Ω/□ [38, 39] and a mobility of 200 000 $cm^2\ V^{-1}\ s^{-1}$ [38], improvements in the quality of CVD-grown graphene can be expected to help realize the tremendous application potential of graphene films. For such improvements, it is critically important to understand the physical properties of CVD-synthesized graphene films and, in particular, the causes that limit their electrical performance.

B H Hong and colleagues recently reported the achievement of 30 Ω/□ sheet resistance in chemically doped four-layer graphene films that were prepared by repeating four individual synthesis and transfer processes [40]. Although this result is notable, the graphene in their study was grown as single-layer films on copper foils [31, 33], resulting in a higher material cost compared to the alternative thin nickel film substrate catalyst [21–30]. Additionally, multiple growth and transfer cycles of single-layer graphene lengthen the film preparation process, limiting the applicability of this method. CVD synthesis of graphene on thin nickel film substrates naturally results in multi-layer graphene and produces a stronger material than the single-layer graphene grown on copper foils. Synthesis on thin nickel film substrates also allows the production of low-resistance films using a simple one-growth, one-transfer process.

This study investigated the morphological properties of CVD-grown graphene films on catalytic nickel substrates, monitoring the evolution of their morphology in response to a change in the methane flow rate during growth. Using atomic force microscopy (AFM), we show that CVD-grown graphene films contain many small peaks with small base areas (small-base-area (SBA) peaks) that are likely composed of amorphous carbon, one of the factors limiting electrical performance. Furthermore, by observing the correlation between the morphologies of the graphene films and the nickel films on which the graphene films were grown, we argue that the SBA peaks on the graphene films originate from corresponding morphological features (small peaks) on the nickel surfaces.

2. Experimental details

2.1. Synthesis and transfer of graphene

Graphene was synthesized on Si/SiO_2 (300 nm)/Ti (20 nm)/Ni (300 nm) substrates purchased from Jinsol, Inc. The

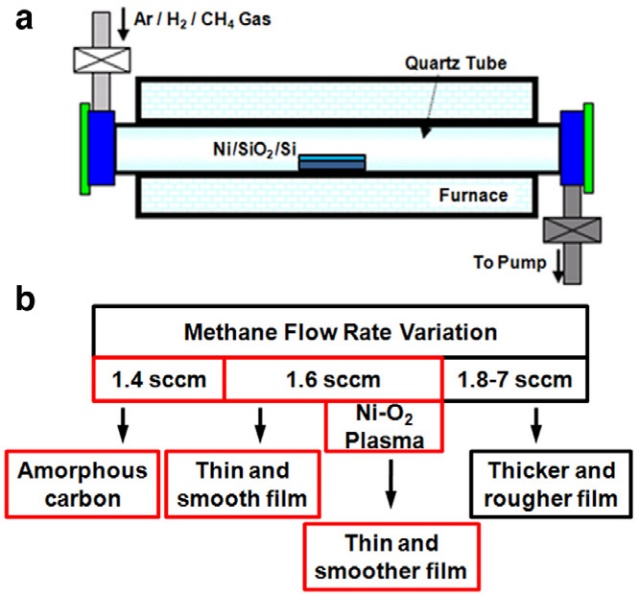

Figure 1. (a) Schematic of the CVD set-up for the synthesis of graphene films. (b) Flowchart summary of our results. Red boxes indicate the synthesis conditions that were studied in detail in this report.

titanium/nickel films were prepared using the DC argon sputtering technique by Jinsol, Inc. For graphene film synthesis, 1 × 1 cm^2 nickel substrates were placed into a chemical vapor deposition (CVD) chamber (figure 1(a)). Then, the chamber was purged with a constant flow of 4 sccm hydrogen and 196 sccm argon for 10 min before setting the pressure to 800 Torr. This flow rate of the gaseous mixture was maintained throughout the CVD procedures. Once the pressure had stabilized, the chamber temperature was raised at a rate of 40 °C min^{-1} to 300 °C. At 300 °C, the temperature was maintained for 30 min as the pre-annealing step, which reduced the presence of the oxidized component on the nickel surface [11]. Next, the temperature was raised to 1000 °C at a rate of 52 °C min^{-1}. When 1000 °C was reached, 200 sccm of hydrogen and 1.4–7 sccm of methane were added to the gas flow for 5 min to grow the graphene films (figure 1(b)). After 5 min, the additional gas flows were closed and the temperature of the CVD chamber was quenched by turning off the heater and opening the cover of the CVD heater box, obtaining an initial cooling rate of more than 200 °C min^{-1} (see supplementary data, figure S1 available at stacks.iop.org/Nano/22/045706/mmedia). Graphene growth occurred as a result of the segregation and precipitation of carbon atoms on the surface and from the inside of the nickel upon saturation and cooling of the nickel substrate, respectively [33]. The use of similar rapid cooling rates has been reported to suppress the formation of thick multiple-layer (ML) domains and induce the formation of thin ML domains [29]. Following synthesis, the graphene film was released from the nickel substrate by etching the nickel in an aqueous iron chloride ($FeCl_3$) solution (1 M) [11]. After washing three times in a distilled water bath, the films were transferred to Si/SiO_2 substrates for analysis and characterization. Si/SiO_2 substrates were used because

Table 1. Properties of the graphene films and the nickel substrates upon which they were synthesized. The graphene films (1.6 sccm) that were grown on annealed nickel substrates (A-Ni) using a methane flow rate of 1.6 sccm showed more SBA peaks and ML domains with smaller areas than the graphene films (1.6 sccm O_2P) grown on nickel substrates that were oxygen-plasma-treated and annealed twice (O_2P–A-Ni) using the same methane flow rate. The 1.6 sccm O_2P graphene films exhibited higher Hall mobility (μ_H) and lower residual charge density (ρ_{2D}) than the 1.6 sccm graphene films.

Sample	Grain area (μm^2)	Sample	No. of SBA peaks	SBA peak area (10^{-3} μm^2)	No. of ML domains	ML domain area (μm^2)	μm (cm^2 V^{-1} s^{-1})	ρ_{2D} (10^{13} cm^{-2})
A-Ni	0.53	1.6 sccm	729 ± 89	13.1 ± 0.5	32 ± 2	3.8 ± 0.5	660 ± 14	1.30 ± 0.04
O_2P–A^2Ni	0.97	1.6 sccm O_2P	492 ± 98	17.3 ± 1.3	23 ± 2	6.2 ± 0.9	770 ± 100	1.14 ± 0.06

of their smooth surface and because their Raman signal does not interfere with that of graphene. Before etching the nickel substrates, a poly(methylmethacrylate) (PMMA) coating was applied as a protective layer and an additional PMMA coating was applied after the graphene/PMMA film was transferred onto the target substrate to improve the transfer process [41]. The second PMMA coating relaxed the graphene/PMMA film so that the graphene films attached more firmly to the substrate, strengthening the graphene films during the removal of the PMMA coating in acetone.

The oxygen plasma treatment of the nickel substrates was performed in a Plasma Oxidation System, HV-100, from Hanvac, Inc. The samples were treated for 6 min in oxygen plasma that was induced by a high-voltage electric source (550 V, 7 mA) in 70 mTorr oxygen.

2.2. Measurements

The atomic force microscope used was an XE-100 system from Park Systems, Inc. Typical AFM scans were performed on a 20×20 μm^2 area at a scan rate of 0.5 Hz in non-contact mode. Raman spectroscopy measurements were performed using an inVia Raman Microscope system from Renishaw, Inc., using a laser equipped with an Ar^+ ion source operating at 514 nm and 10 mW. Hall measurements were performed using a Hall measurement system from Bio-Rad, Inc.

3. Results and discussion

3.1. Evolution of graphene film morphology with methane flow rate

We first investigated the relationship between the morphological evolution of graphene films and the methane flow rate during CVD synthesis. The graphene films were synthesized using various methane flow rates, from 1.4 to 7 sccm, while keeping the other parameters constant. Similar to previous results [23, 29], we found that the graphene film did not form at a methane gas flow rate of 1.4 sccm; instead, films consisting of lumped amorphous carbon were formed. With methane flow rates of 1.6 sccm and above, graphene films were formed that contained single-layer (SL), double-layer (DL) and multiple-layer (ML) domains. As discussed in detail below and in supplementary data,(available at stacks.iop.org/Nano/22/045706/mmedia) the graphene films synthesized at the higher flow rate were thicker and rougher, because the higher methane flow allowed more carbon source to be absorbed into the nickel catalyst.

AFM was used to survey the morphological features of the graphene films, including film thickness and surface roughness (see supplementary data figures S3–S5 available at stacks.iop.org/Nano/22/045706/mmedia). The 1.6 sccm graphene film exhibited the best morphology for electrode applications, with a thickness of 3.4 $\pm$ 0.2 nm and an rms roughness of 2.2 $\pm$ 0.1 nm. Kong and colleagues primarily used optical characterization methods to determine that the methane flow rate that grows the morphologically optimal graphene film is that just above the rate that does not grow a graphene film [29].

Hall probe measurements [42] also indicated that the 1.6 sccm graphene film was optimal (see supplementary data, figure S5 available at stacks.iop.org/Nano/22/045706/mmedia). The 1.6 sccm graphene film showed the highest Hall mobility (660 ± 14 cm^2 V^{-1} s^{-1}) among graphene films prepared with different methane flow rates and had a low residual charge density ($+1.30 \pm 0.04 \times 10^{13}$ cm^{-2}; table 1).

In the following section, the morphological features observed on the 1.6 sccm graphene and 1.4 sccm amorphous carbon films are discussed in more detail. The correspondence between the surface morphology of these films and that of the nickel catalysts is also discussed.

3.2. Correspondence between graphene film and nickel substrate morphologies

AFM measurements demonstrated that the graphene films exhibited small-base-area peaks (SBA peaks) with heights of tens of nanometers (figure 2 and figures S3 and S4 in supplementary data available at stacks.iop.org/Nano/22/045706/mmedia). Because the typical length of the base area was of the order of 100 nm, these peaks were not visible under an optical microscope (see supplementary data, figure S2 available at stacks.iop.org/Nano/22/045706/mmedia). This observation is the first report to mention the existence of the SBA peaks on CVD-synthesized graphene films on nickel substrates [22–30]. Because our synthesis method is similar to those of other groups [22–30], it is highly likely that the SBA peaks exist commonly on graphene films synthesized on nickel substrates. The presence of these high peaks can be problematic for electrode applications because some organic electronic devices have very thin active layers [43, 44]. Therefore, it is important to understand the origin and material identity of these SBA peaks.

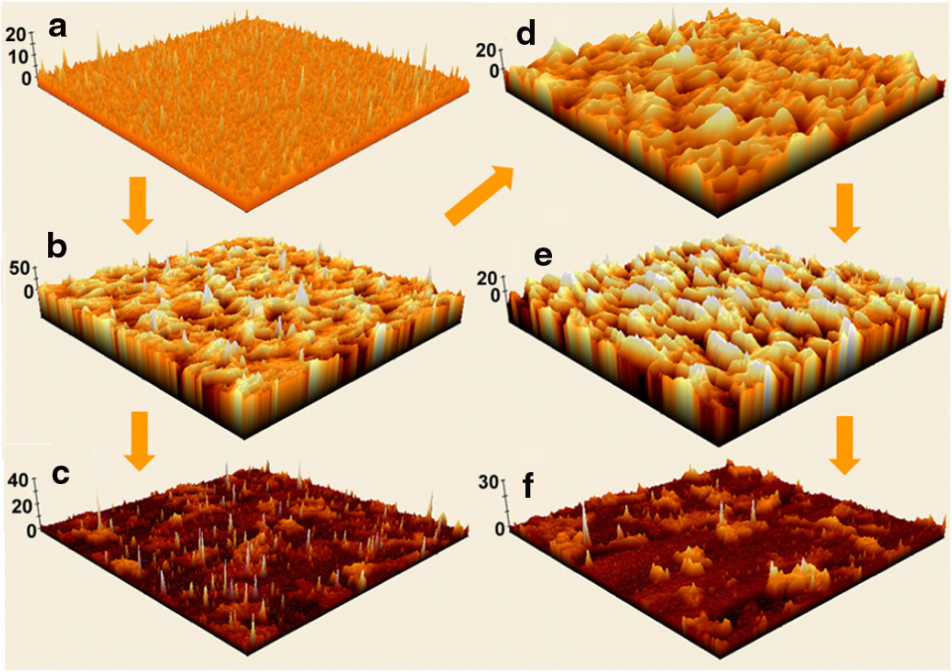

Figure 2. AFM images from (a) an as-prepared nickel substrate, (b) a thermally annealed nickel substrate, (c) a graphene film synthesized on a nickel substrate similar to (b), (d) a nickel substrate after thermal annealing and oxygen plasma treatment, (e) a nickel substrate annealed a second time after oxygen plasma treatment and (f) a graphene film synthesized on a nickel substrate similar to (e). All images have an area of $20 \times 20\ \mu m^2$ and the vertical axes are scaled in nanometers.

To investigate the origin of the SBA peaks, we probed the nickel substrates. As shown in figure 2, the as-prepared nickel substrates contain many small peaks and grains with areas of approximately $6.8 \times 10^{-2}\ \mu m^2$ (figure 2(a), and see also supplementary data, figure S7 available at stacks.iop.org/Nano/22/045706/mmedia). When the nickel substrates were annealed with the same thermal cycles as those used for the graphene synthesis (denoted as A-Ni), the numerous small peaks coalesced into fewer peaks with greater heights (figure 2(b)) and the grain size increased eightfold to approximately $0.53\ \mu m^2$ (figure 3(b), and see also supplementary data, figure S7 available at stacks.iop.org/Nano/22/045706/mmedia). The distribution and shape of the small peaks on the A-Ni surface were similar to those of the SBA peaks on the graphene films (figures 2(b) and (c)). Therefore, we speculate that the small peaks on A-Ni are the origin of the SBA peaks on the graphene films.

To verify this assumption, we modified the morphology of the A-Ni substrate by oxygen plasma etching. Most of the small peaks diminished after etching, as shown in figure 2(d). When the etched nickel substrate was reannealed using the thermal cycles (denoted as O_2P–A-Ni), fewer peaks with smaller heights were observed compared to the A-Ni surface and the grain size increased twofold to approximately $0.97\ \mu m^2$ (figure 2(e) and supplementary data, figure S7 available at stacks.iop.org/Nano/22/045706/mmedia). Corresponding to the change in surface morphology of the Ni substrate, the graphene films synthesized on the O_2P–A-Ni substrate possessed fewer SBA peaks with smaller heights (figure 2(f)) than those synthesized on the A-Ni substrate (figure 2(c)).

To statistically verify this observation, we used AFM to characterize three 1.6 sccm graphene samples synthesized on the O_2P–A-Ni substrate (1.6 sccm O_2P graphene) in the same manner as described in the supplementary data (available at stacks.iop.org/Nano/22/045706/mmedia). The average thickness and rms roughness of the 1.6 sccm O_2P graphene films were 3.6 ± 0.2 nm and 2.0 ± 0.1 nm, respectively. Detailed analyses indicate that, compared to the 1.6 sccm graphene, the number of SBA peaks in the 1.6 sccm O_2P graphene decreased by 33%, to 492 ± 98 peaks from 729 ± 89 peaks, and the number of ML domains also decreased while the average ML domain area increased (table 1). For the analysis, the threshold method of the grain-detecting function of the XEI program (Park Systems, Inc.) was used to detect domains higher than 2 nm (see supplementary data, figure S3 available at stacks.iop.org/Nano/22/045706/mmedia). Areas detected with lengths below 1 μm were counted as SBA peaks and the remainder were categorized as ML domains. The increase in ML domain size can be attributed to the larger grain sizes of the O_2P–A-Ni substrates; similar results have been reported elsewhere [24, 30]. Therefore, we observed two morphological correspondences between the nickel substrates and the graphene films synthesized on them: (1) the number of SBA peaks decreased as the number of small peaks on the nickel substrate decreased and (2) the average area of the ML domains increased as the grain size on the nickel substrate increased. The ability to reduce the formation of SBA peaks on graphene films by modifying the nickel substrate surface is an interesting result that might enable wider application of CVD-synthesized graphene films as electrodes in electronic devices with thin active layers [43, 44].

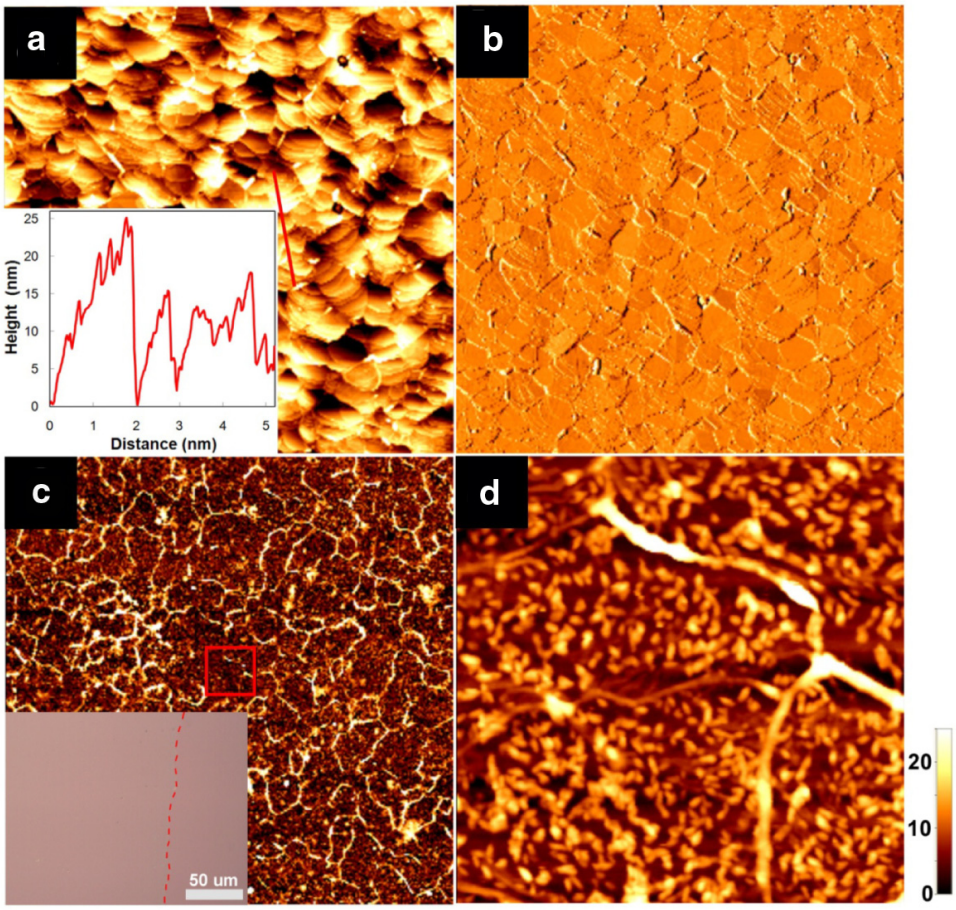

Figure 3. Morphological features of the 1.4 sccm carbon film and nickel substrate. (a) An AFM image of an annealed nickel substrate, demonstrating slanted grains with lengths of several microns. The inset shows the height profile along the red line. (b) The grain boundaries in (a) can be observed more clearly by showing the difference between the forward and backward scan signals. ((c), (d)) AFM images of a 1.4 sccm carbon film deposited onto an SiO_2 substrate. Amorphous carbon ridges with heights of tens of nanometers were formed along the grain boundaries of the nickel substrate. The inset in (c) shows an optical micrograph of a 1.4 sccm carbon film. The red dashed line marks the border between the carbon film (left) and the SiO_2 substrate (right). (d) A detailed scan image of the red squared area in (c). Panels (c) and (d) have the same vertical color scale bar (in nm), as indicated near (d). All images represent areas of 20×20 μm^2, except (d), which represents an area of 2×2 μm^2.

The morphological correspondence with the nickel substrate was also observed in 1.4 sccm carbon films. As shown in the inset of figure 3(c) and also in figure S2(a) in the supplementary data (available at stacks.iop.org/Nano/22/045706/mmedia), these carbon films were barely visible under the optical microscope. However, the AFM images indicated that these films were not continuous films, but were aggregations of small lumps and ridges, as shown in figures 3(c) and (d). The ridges were formed along the grain boundaries of the nickel substrate, as seen by comparing figures 3(b) and (c).

The micro-Raman spectroscopy measurements shown in figure 4(a) were used to identify the material of the 1.4 sccm carbon film as amorphous carbon. The Raman measurements were performed on 4×4 spots of 2 μm diameter that were separated by 5 μm in both the x and y directions. Figure 4(a) shows a representative Raman spectrum. We observed a narrow peak near 2300 cm^{-1} that is known to appear in sp^3-rich amorphous carbon and a broad peak near 2900 cm^{-1} that is known to appear in sp^3-poor amorphous carbon [45]. The features observed near and below 1500 cm^{-1} arise from the combined features of amorphous carbon and the SiO_2 substrate [45–48]. Because amorphous carbon possesses a much smaller scattering cross section to the source light, the observed Raman signal intensity (figure 4(a)) is an order of magnitude smaller than the Raman signal intensities observed in the graphene samples (figures 4(b)–(d)) [45]. Likewise, the amorphous carbon film is less visible under optical microscopy.

We considered why amorphous carbon lumps and ridges rather than graphene films formed at the 1.4 sccm methane flow rate. At this flow rate, the amount of carbon absorbed into the nickel catalyst was not sufficient to form a continuous graphene film. Instead, the absorbed carbon predominantly precipitated on high-curvature surface areas, such as the small peaks and grain boundaries on the nickel substrate due to the Gibbs–Thomson effect (i.e. denser precipitation on curved surfaces) [49]. In the high-curvature areas, precipitated carbon may have formed amorphous carbon due to the lack of available catalyst surface to induce graphene formation.

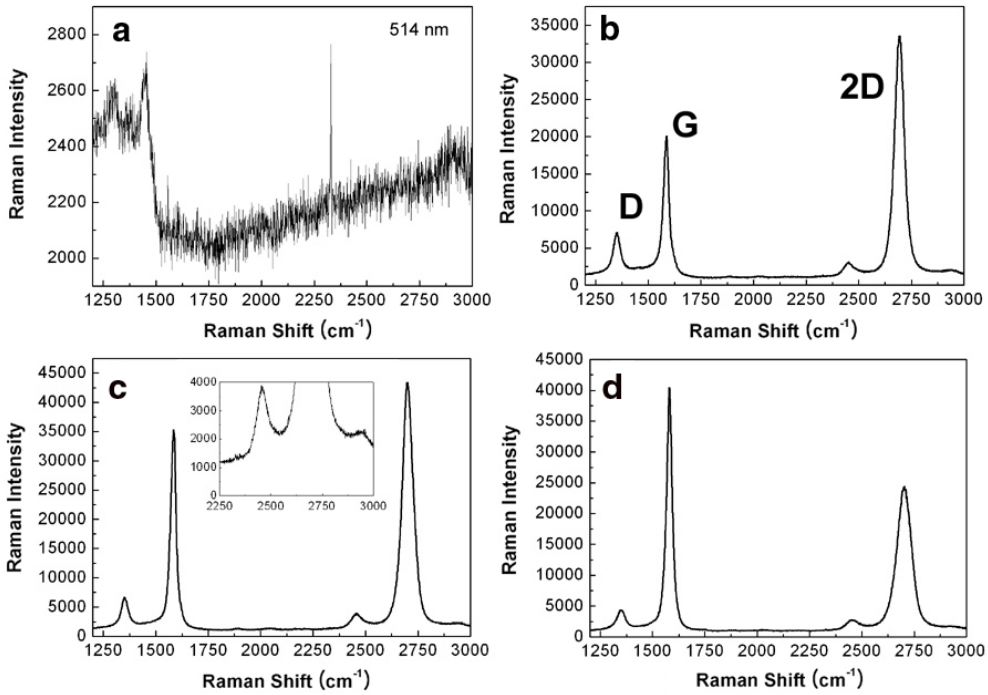

Figure 4. Raman spectra of CVD-synthesized carbon and graphene films. Raman spectra of (a) a 1.4 sccm carbon film and ((b)–(d)) a 1.6 sccm graphene film showing Raman signal features from (b) SL, (c) DL and (d) ML domains. The inset in (c) clearly shows the broad peak near 2900 cm^{-1} that exists in ((b)–(d)).

Similarly, because of the lumped shapes, we speculate that the SBA peaks observed on the graphene films are also made up of amorphous carbon that originated from small peaks on the nickel substrate. The small peaks on the nickel catalyst may induce SBA peaks of amorphous carbon nature on the graphene film for reasons similar to those explained above. The graphene film is mainly formed by the precipitation of absorbed carbon onto the nickel catalyst as the nickel cools [33]. When the nickel catalyst cools, absorbed carbon precipitates densely, likely forming amorphous carbon in the small peak regions of the nickel substrate. The existence of amorphous carbon on graphene films was verified using Raman spectroscopy, as discussed below.

We verified the formation of graphene films when using methane flow rates of 1.6 sccm or higher using micro-Raman spectroscopy (figures 4(b)–(d)). The same micro-Raman measurement protocol used on the 1.4 sccm carbon film was used on the graphene films. All measured graphene samples displayed well-known D-band peaks near 1350 cm^{-1}, G-band peaks near 1580 cm^{-1} and 2D-band peaks near 2700 cm^{-1}, indicative of graphene [45]. Figures 4(b)–(d) show representative Raman spectra taken of the 1.6 sccm graphene sample. The number of graphene layers can be estimated from the ratio of the G- and 2D-peak heights, although this ratio is affected by the residual charge density and defect density [45, 50–52]. The spectra shown in figures 4(b)–(d) are thus categorized as arising from the SL, DL and ML domains, respectively. It appears that, when a sufficient amount of carbon is absorbed in the nickel substrate, most of the precipitated carbon forms sp^2-bonded graphene as the substrate cools. Sp^2-bonded graphene is energetically more favorable than sp^3-rich amorphous carbon [53, 54]. However, some of the precipitated carbon remained as amorphous carbon, as observed in the spectra shown in figures 4(b)–(d). These spectra exhibited the Raman signature of sp^3-poor amorphous carbon, i.e. broad peaks near 2900 cm^{-1} (see the inset in figure 4(c)). These Raman spectroscopic measurements confirmed the formation of graphene and the existence of amorphous carbon in our CVD-synthesized graphene films. The amorphous carbon most likely exists as the SBA peaks that were observed using the AFM measurements of the graphene films and 1.4 sccm carbon films.

The existence of amorphous carbon on the CVD-synthesized graphene films was further confirmed by detailed Raman spectroscopy mapping. For these measurements, the 1.6 sccm graphene film and 1.6 sccm O_2P graphene film were scanned in 20 × 20 μm^2 areas with a 2 μm diameter laser spot at 1 μm intervals in both the x and y directions, obtaining 21 × 21 Raman spectra of each sample. These spectra were used to produce the analytical Raman mapping images shown in figure 5, which presents the results from the 1.6 sccm O_2P graphene (see supplementary data, figure S8 available at stacks.iop.org/Nano/22/045706/mmedia, for the results from the 1.6 sccm graphene sample). The graphene film contained SL, DL and ML domains, as shown in figure 5(a). Figure 5(b) plots the ratios of the D- to G-peak areal intensities that are known to be proportional to the defect density in the graphene film [45]. Interestingly, we observed that the defect density in the graphene film is inversely proportional to the number of layers by comparing figures 5(a) and (b). That is, the SL domains showed higher defect densities than did the ML domains. The higher D-peak intensity in the SL domains may

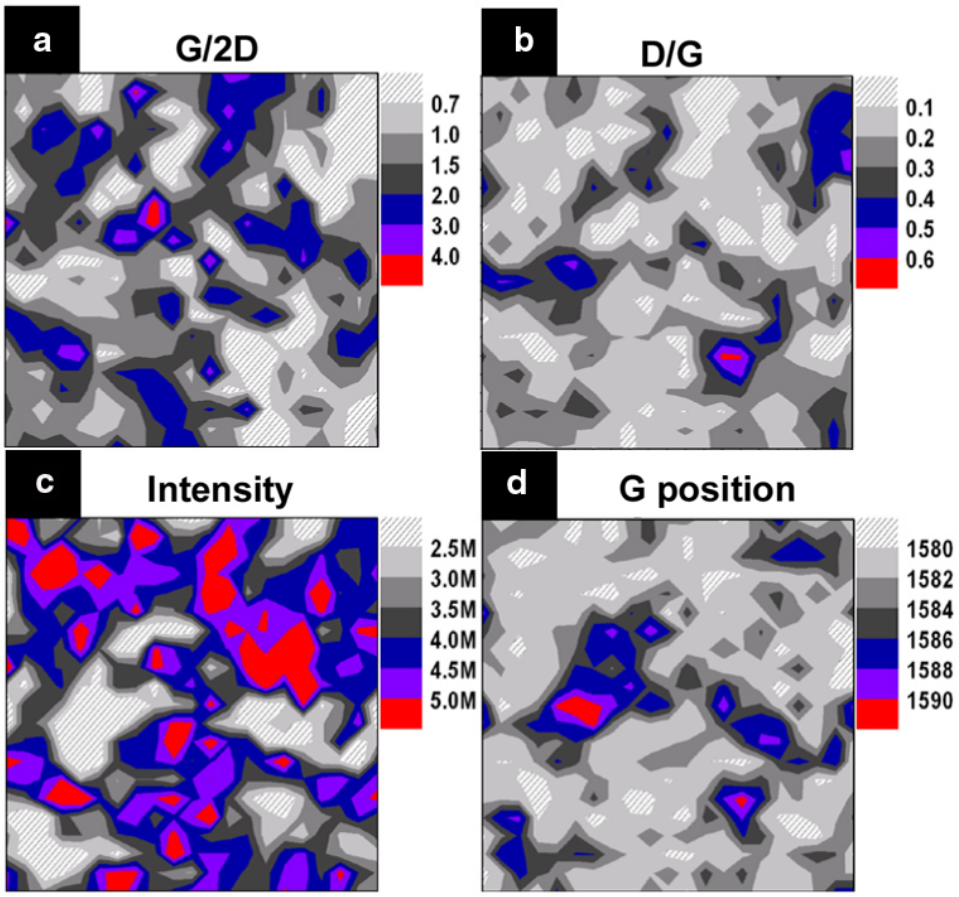

Figure 5. Raman analysis mapping images from a 1.6 sccm O_2P graphene film. These mapping images show 21 × 21 spots of 2 μm diameter at 1 μm intervals in both the x and y directions. (a) The mapping image of the G-peak/2D-peak height ratios indicating the number of graphene layers, where values below 0.7 indicate ∼ single layers, values between 0.7 and 1.0 indicate ∼ double layers, and values above 1.0 indicate multiple layers. (b) The mapping image of the D-peak/G-peak areal ratios, which are proportional to the defect density. (c) The Raman total intensities (these are proportional to the amount of graphitic material). (d) The G-peak positions (cm^{-1}, these blueshift with increasing residual charge density).

have been induced because the interaction with the underlying SiO_2 substrate that induces the D-peak signal [55] was stronger due to the graphene film being thinner in these domains.

The Raman intensity maps, shown in figure 5(c), were obtained by summing the areal intensities of the D, G and 2D bands of the Raman spectra. This intensity is proportional to the amount of graphitic material. Interestingly, the amount of graphitic material, shown in figure 5(c), was not necessarily proportional to the number of graphene layers, shown in figure 5(a). If all precipitated carbon was part of the graphene film, then the Raman signal intensity would be proportional to the number of graphene layers, i.e. the ML domains would show a higher intensity than the SL domains. The poor correspondence between the number of layers and the degree of graphitization can be attributed to the presence of amorphous carbon. For example, in the upper right corner of these images, there is a SL domain with a high degree of graphitization. In the lower right corner, however, there is also a SL domain, but it has a low degree of graphitization due to the presence of amorphous carbon.

We speculated that amorphous carbon exists as SBA peaks on graphene films. This speculation is also supported by comparing figures 5(c) and (d). Figure 5(d) maps the G-peak positions. The G-peak position blueshifts sensitively as the residual charge density increases [52]. This comparison indicates that areas of poor graphitization showed high residual charge densities (as an example, compare the middle left areas of the two images). This observation can be explained by the presence of SBA amorphous carbon peaks in poorly graphitized areas. Because the surface in areas with SBA peaks is significantly rougher, more gas molecules can adsorb, consequently increasing the residual charge density in these areas.

The detailed Raman scan results of the 1.6 sccm graphene and 1.6 sccm O_2P graphene samples yielded the analytical plots depicted in figure 6. The dependence of the D-peak intensity on the number of graphene layers is shown in figure 6(a). The G-peak position also depends on the number of layers to some extent, redshifting as the number of layers increases as shown in figure 6(b) [50]. The total Raman intensity weakly increased as the number of layers increased (figure 6(c)). Comparing the plotted data of the two graphene samples, we observed that, in the 1.6 sccm O_2P graphene, the defect density and residual charge density decreased as

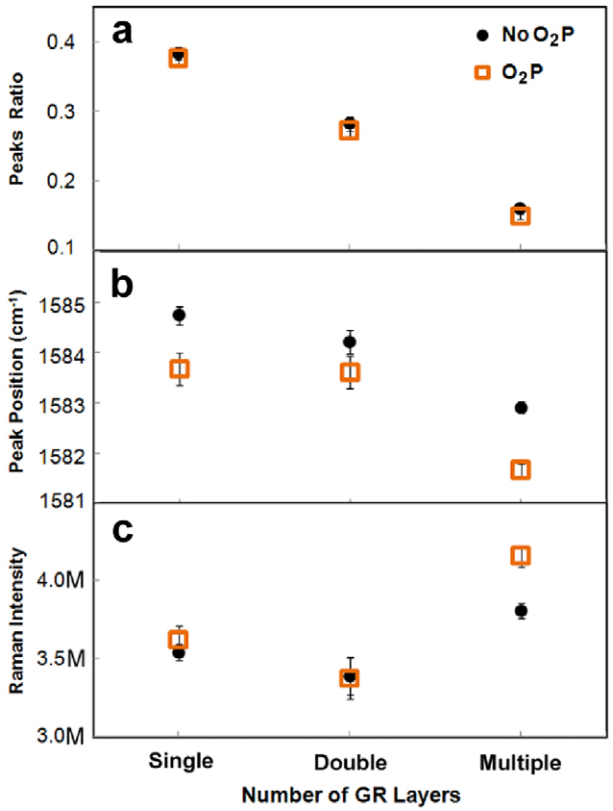

Figure 6. Raman analysis plots of the data from figure 6 and figure S6 in the supplementary data (available atstacks.iop.org/Nano/22/045706/mmedia). The averages of (a) D-peak/G-peak areal ratios, (b) G-peak positions and (c) Raman total intensities from SL, DL and ML domains are plotted.

graphitization increased. These observations are consistent with the fact that the 1.6 sccm O_2P graphene film contained fewer SBA carbon peaks (probably of amorphous carbon nature) than the 1.6 sccm graphene film.

Finally, we investigated the electrical properties of the 1.6 sccm graphene and 1.6 sccm O_2P graphene samples. The Hall mobilities and residual charge densities of these films are listed in table 1. We observed that the Hall mobility of the graphene film increased as the number of SBA peaks decreased. This increase can be understood by considering that SBA peaks can act as scattering centers for the conducting electrons. We can estimate the expected increase in the mobility given the decrease in the number of SBA peaks. Our CVD-synthesized graphene films consist of SL, DL and ML domains. Because the observed defect densities are different in these domains, the mobility would also be different; the highest mobility would be in the ML domains, which have the smallest defect densities. The formula used to combine the electron or hole mobilities (μ) from two regions of the same width in a series is $1/\mu = 1/\mu_1 \times w_1 + 1/\mu_2 \times w_2$, where μ_1 and μ_2 are the electron or hole mobilities of different regions, and w_1 and w_2 are the weighting factors determined by the area of each region [56]. This equation indicates that regions of lower mobility and larger area contribute more strongly to the combined mobility. In our graphene films, the ML domains possess approximately 30% of the area and have the highest expected mobility. Therefore, to simplify the analysis, we assumed that only the SL and DL domains contribute to the film mobility by their average mobility μ_{SD}. Next, because the mobility is proportional to the mean free path (λ), we calculated the change in λ relative to the change in the number of SBA peaks. The average areas (A) around a single SBA peak in the two samples are $A(1.6\ \text{sccm}) = (400 - 3.8 \times 32)\ \mu\text{m}^2/729 = 0.382\ \mu\text{m}^2$ and $A(1.6\ \text{sccm}\ O_2P) = 0.523\ \mu\text{m}^2$ (table 1). The contribution of the SBA peaks to the mean free path is proportional to the square root of the average areas; therefore, $\lambda(1.6\ \text{sccm}\ O_2P)/\lambda(1.6\ \text{sccm}) = 0.723/0.618 = 1.17$. This result indicates that a 17% increase in the mean free path or a 17% increase in the mobility is expected from the observed decrease in the number of SBA peaks. This value agrees with the observed increase in the Hall mobility of 17% ($\mu_H(1.6\ \text{sccm}\ O_2P)/\mu_H(1.6\ \text{sccm}) = 770/660 = 1.17$). Our calculations for the change in the mobility assume that the dominant scattering factor affecting the mobility is the scattering by the SBA peaks, which needs further justification. Therefore, the observed agreement between the expected and observed increases in the mobility could be accidental. However, our calculations reveal a correlation between the number of SBA peaks and the Hall mobility in these CVD-synthesized graphene films.

4. Conclusions

In conclusion, we investigated in detail graphene films that were synthesized by the chemical vapor deposition (CVD) method on nickel catalytic substrates. We found that the graphene films contained numerous small-base-area (SBA) peaks probably composed of amorphous carbon that were induced by similarly shaped small peaks on the nickel substrates. These SBA peaks were found to be one of the reasons for the inferior electrical properties of CVD-synthesized graphene films compared to those of graphene films prepared by other methods. We demonstrated that these undesirable SBA peaks could be suppressed by controlling the surface morphology of the nickel substrate, which may be a useful finding for the development of methods to synthesize high-quality, large-area graphene films using CVD.

Acknowledgments

This work was supported by the National Research Laboratory (NRL) Program, a National Core Research Center (NCRC) grant, the World Class University (WCU) program of the Korean Ministry of Education, Science and Technology (MEST), the Program for Integrated Molecular System, and the Core Technology Development Program for next-generation solar cells of the Research Institute for Solar and Sustainable Energies (RISE) at GIST.

References

[1] Geim A K and Novoselov K S 2007 *Nat. Mater.* **6** 183–91
[2] Geim A K 2009 *Science* **324** 1530–4
[3] Wassei J K and Kaner R B 2010 *Mater. Today* **13** 52–9
[4] Blake P *et al* 2008 *Nano Lett.* **8** 1704–8

[5] Liu J, Yin Z, Cao X, Zhao F, Lin A, Xie L, Fan Q, Boey F, Zhang H and Huang W 2010 *ACS Nano* **4** 3987–92
[6] Di C-a, Wei D, Yu G, Liu Y, Guo Y and Zhu D 2008 *Adv. Mater.* **20** 3289–93
[7] Lee C-G, Park S, Ruoff R S and Dodabalapur A 2009 *Appl. Phys. Lett.* **95** 023304
[8] Pang S, Tsao H N, Feng X and Müllen K 2009 *Adv. Mater.* **21** 3488–91
[9] Wu J, Agrawal M, Becerril H c A, Bao Z, Liu Z, Chen Y and Peumans P 2009 *ACS Nano* **4** 43–8
[10] Sun T, Wang Z L, Shi Z J, Ran G Z, Xu W J, Wang Z Y, Li Y Z, Dai L and Qin G G 2010 *Appl. Phys. Lett.* **96** 133301–3
[11] Jo G *et al* 2010 *Nanotechnology* **21** 175201
[12] Matyba P, Yamaguchi H, Eda G, Chhowalla M, Edman L and Robinson N D 2010 *ACS Nano* **4** 637–42
[13] Wang X, Zhi L and Müllen K 2008 *Nano Lett.* **8** 323–7
[14] Wang X, Zhi L, Tsao N, Tomović Ž, Li J and Müllen K 2008 *Angew. Chem. Int. Edn* **47** 2990–2
[15] Wu J, Becerril H A, Bao Z, Liu Z, Chen Y and Peumans P 2008 *Appl. Phys. Lett.* **92** 263302
[16] Wang Y, Chen X, Zhong Y, Zhu F and Loh K P 2009 *Appl. Phys. Lett.* **95** 063302
[17] Gomez De Arco L, Zhang Y, Schlenker C W, Ryu K, Thompson M E and Zhou C 2010 *ACS Nano* **4** 2865–73
[18] Park S and Ruoff R S 2009 *Nat. Nanotechnol.* **4** 217–24
[19] Eda G and Chhowalla M 2010 *Adv. Mater.* **22** 2392–415
[20] Yamaguchi H, Eda G, Mattevi C, Kim H and Chhowalla M 2010 *ACS Nano* **4** 524–8
[21] Eizenberg M and Blakely J M 1979 *Surf. Sci.* **82** 228–36
[22] Kim K S, Zhao Y, Jang H, Lee S Y, Kim J M, Kim K S, Ahn J-H, Kim P, Choi J-Y and Hong B H 2009 *Nature* **457** 706–10
[23] Chae S J *et al* 2009 *Adv. Mater.* **21** 2328–33
[24] Reina A, Jia X, Ho J, Nezich D, Son H, Bulovic V, Dresselhaus M S and Kong J 2009 *Nano Lett.* **9** 30–5
[25] Yu Q, Lian J, Siriponglert S, Li H, Chen Y P and Pei S-S 2008 *Appl. Phys. Lett.* **93** 113103
[26] Gomez De Arco L, Zhang Y, Kumar A and Zhou C 2009 *IEEE Trans. Nanotechnol.* **8** 135–8
[27] Lee Y, Bae S, Jang H, Jang S, Zhu S-E, Sim S H, Song Y I, Hong B H and Ahn J-H 2010 *Nano Lett.* **10** 490–3
[28] Zheng M *et al* 2010 *Appl. Phys. Lett.* **96** 063110
[29] Reina A, Thiele S, Jia X, Bhaviripudi S, Dresselhaus M, Schaefer J and Kong J 2009 *Nano Res.* **2** 509–16
[30] Thiele S, Reina A, Healey P, Kedzierski J, Wyatt P, Hsu P-L, Keast C, Schaefer J and Kong J 2010 *Nanotechnology* **21** 015601
[31] Li X *et al* 2009 *Science* **324** 1312–4
[32] Levendorf M P, Ruiz-Vargas C S, Garg S and Park J 2009 *Nano Lett.* **9** 4479–83
[33] Li X, Cai W, Colombo L and Ruoff R S 2009 *Nano Lett.* **9** 4268–72
[34] Ismach A, Druzgalski C, Penwell S, Schwartzberg A, Zheng M, Javey A, Bokor J and Zhang Y 2010 *Nano Lett.* **10** 1542–8
[35] Kim J Y, Lee K, Coates N E, Moses D, Nguyen T-Q, Dante M and Heeger A J 2007 *Science* **317** 222–5
[36] Park S H, Roy A, Beaupré S, Cho S, Coates N, Moon J S, Moses D, Leclerc M, Lee K and Heeger A J 2009 *Nat. Photon.* **3** 297–303
[37] Chen H-Y, Hou J, Zhang S, Liang Y, Yang G, Yang Y, Yu L, Wu Y and Li G 2009 *Nat. Photon.* **3** 649–53
[38] Chen J-H, Jang C, Xiao S, Ishigami M and Fuhrer M S 2008 *Nat. Nanotechnol.* **3** 206–9
[39] De S and Coleman J N 2010 *ACS Nano* **4** 2713–20
[40] Bae S *et al* 2010 *Nat. Nanotechnol.* **5** 574–8
[41] Li X, Zhu Y, Cai W, Borysiak M, Han B, Chen D, Piner R D, Colombo L and Ruoff R S 2009 *Nano Lett.* **9** 4359–63
[42] van der Pauw L J 1958 *Philips Res. Rep.* **13** 1–9
[43] Cho B, Kim T-W, Song S, Ji Y, Jo M, Hwang H, Jung G-Y and Lee T 2010 *Adv. Mater.* **22** 1228–32
[44] Ji Y, Cho B, Song S, Kim T W, Choe M, Kahng Y H and Lee T 2010 *Adv. Mater.* **22** 3071–5
[45] Ferrari A C 2007 *Solid State Commun.* **143** 47–57
[46] Yoshikawa M, Katagiri G, Ishida H, Ishitani A and Akamatsu T 1988 *Solid State Commun.* **66** 1177–80
[47] Mikkelsen J C Jr and Galeener F L 1980 *Appl. Phys. Lett.* **37** 712–4
[48] Geissberger A E and Galeener F L 1983 *Phys. Rev.* B **28** 3266–71
[49] Shahandeh S and Nategh S 2007 *Mater. Sci. Eng.* A **443** 178–84
[50] Graf D, Molitor F, Ensslin K, Stampfer C, Jungen A, Hierold C and Wirtz L 2007 *Nano Lett.* **7** 238–42
[51] Casiraghi C, Pisana S, Novoselov K S, Geim A K and Ferrari A C 2007 *Appl. Phys. Lett.* **91** 233108
[52] Das A *et al* 2008 *Nat. Nanotechnol.* **3** 210–5
[53] Reznik A, Richter V and Kalish R 1997 *Phys. Rev.* B **56** 7930–4
[54] Kahng Y H, Choi J, Park B C, Kim D-H, Choi J-H, Lyou J and Ahn S J 2008 *Nanotechnology* **19** 195705
[55] Ishigami M, Chen J H, Cullen W G, Fuhrer M S and Williams E D 2007 *Nano Lett.* **7** 1643–8
[56] Sze S M and Ng K K 2007 *Physics of Semiconductor Devices* (Hoboken, NJ: Wiley)